Adsorption and photocatalytic oxidation of ibuprofen using nanocomposites of TiO2 nanofibers combined with BN nanosheets: Degradation products and mechanisms

Lu Lin, Wenbin Jiang, Mikhael Bechelany, Maryline Nasr, Jacqueline Jarvis, Tanner Schaub, Rishi Sapkota, Philippe Miele, Huiyao Wang, Pei Xu

1 **Adsorption and photocatalytic oxidation of ibuprofen using nanocomposites of TiO₂**

2 **nanofibers combined with BN nanosheets: degradation products and mechanisms**

3

4 Lu Lin[1], Wenbin Jiang[1], Mikhael Bechelany[2], Maryline Nasr[2], Jacqueline Jarvis[3], Tanner

5 Schaub[3], Rishi R. Sapkota[3], Philippe Miele[2], Huiyao Wang[4*], Pei Xu[1*]

6

7 [1]Department of Civil Engineering, New Mexico State University, 3035 S Espina Street, Las

8 Cruces, NM 88003, USA

9 [2]Institut Européen des Membranes, IEM, UMR-5635, Université de Montpellier, ENSCM,

10 CNRS, Place Eugène Bataillon, F-34095 Montpellier Cedex 5, France

11 [3]Chemical Analysis and Instrumentation Laboratory, College of Agricultural, Consumer and

12 Environmental Sciences, New Mexico State University, Las Cruces, NM 88003, USA

13 [4]Core University Research Resources Laboratory, New Mexico State University, Las Cruces,

14 NM 88003, USA

15

16 [*]Corresponding author: Dr. Huiyao Wang, Email: huiyao@nmsu.edu

17 [*]Corresponding author: Dr. Pei Xu, Email: pxu@nmsu.edu

18

19

20   **Abstract**

21   This study investigated the adsorption and photocatalytic activity of TiO_2-boron nitride (BN)

22   nanocomposites for the removal of contaminants of emerging concern in water using ibuprofen

23   as a model compound. TiO_2 nanofibers wrapped by BN nanosheets were synthesized by

24   electrospinning method. Characterization of the nanocomposite photocatalysts indicated the BN

25   nanosheets improved the light absorbance and reduced the recombination of the photoexcited

26   charge carriers (e^- and h^+). The photocatalytic oxidation products and mechanisms of ibuprofen

27   by the TiO_2-BN catalysts were elucidated using a multiple analysis approach by high

28   performance liquid chromatography, ultraviolet absorbance, dissolved organic carbon,

29   fluorescence excitation-emission matrices, and electrospray ionization–liquid chromatography–

30   tandem mass spectrometry. The experimental results revealed that the photocatalytic oxidation

31   by the TiO_2-BN nanocomposites is a multi-step process and the interactions between ibuprofen

32   molecules and the TiO_2-BN nanocomposites govern the adsorption process. The increasing BN

33   nanosheet content in the TiO_2 nanofibers facilitated the breakdown of ibuprofen degradation

34   intermediates (hydroxyibuprofen, carboxyibuprofen, and oxypropyl ibuprofen). Kinetic

35   modeling indicated both adsorption and photocatalytic oxidation of ibuprofen by the TiO_2-BN

36   nanocomposites followed the first-order kinetic model. The photocatalytic oxidation rate

37   increased with the increasing BN content in the nanocomposite catalysts, which was attributed to

38   the light absorption capacity and the separation efficiency of the photoexcited electron (e^-)-hole

39   (h^+) pairs. Multiple photocatalytic cycles were conducted to investigate the reusability and

40   regeneration of the nanofibers for degradation of ibuprofen.

41

1. Introduction

Contaminants of emerging concerns such as pharmaceuticals and personal care products (PPCPs) have been widely detected in water bodies around the world (Vieno et al., 2007). Many PPCPs are of serious concerns even in trace amounts due to their toxicity to aquatic life and potential risks to public health (Vieno et al., 2007; Christen et al., 2010). Conventional water and wastewater treatment processes including coagulation, sedimentation, media filtration, and biological processes are not effective to remove these recalcitrant organic contaminants (Vieno et al., 2007; Xiang et al., 2016). Adsorption by activated carbon is an efficient technique to remove hydrophobic PPCPs through hydrophobic interactions, however the adsorption capacity gradually decreases as the carbon is saturated with the adsorbed chemicals. In addition, it is ineffective to adsorb hydrophilic compounds such as atenolol, acetaminophen, and naproxen (Vieno et al., 2007; Huerta-Fontela et al., 2011; Wang et al., 2015). Oxidation using chlorine, chlorine dioxide, and ozone is typically effective to degrade PPCPs with electron-donating functional groups (e.g., phenolic-and amine-containing compounds) (Lee and von Gunten, 2010). Ultraviolet (UV) irradiation can degrade many PPCPs but treatment cost is inhibitive because of high energy demand (Rosenfeldt and Linden, 2004).

To degrade the persistent organic contaminants, advanced oxidation processes (AOPs) are typically needed (De la Cruz et al., 2012). AOPs generate hydroxyl radicals ($\cdot$OH) which react non-selectively with most organic compounds (Andreozzi et al., 1999). Commonly used AOPs for PPCPs removal from wastewater include UV/H_2O_2, UV/O_3, (photo)-Fenton, and heterogeneous photocatalysis (De Witte et al., 2009; Homem and Santos, 2011; Prieto-Rodriguez et al., 2012; Carbonaro et al., 2013; Van Doorslaer et al., 2015; Thagard et al., 2016). Complete mineralization is usually not the goal of AOPs because it is energy intensive and not cost-

effective (Doll and Frimmel, 2004). Partial degradation of recalcitrant PPCPs is more economically attractive to deactivate their biological activity or increase their biodegradability (Van Doorslaer et al., 2015). But more concerns are raised regarding the intermediate degradation products and their environmental toxicities.

Heterogeneous photocatalytic oxidation using metal oxides (e.g., TiO_2) has attracted considerable attention particularly due to its potentially lower cost than other AOPs (Jing et al., 2006; Dalrymple et al., 2007; Rubio et al., 2013; Lin et al., 2015; Arlos et al., 2016; Lin et al., 2016; Lin et al., 2017b; Lin et al., 2017f; Li and Hu, 2018). More than 90 organic and 25 inorganic compounds catalogued on the US Environmental Protection Agency's (USEPA) priority list of contaminants have been investigated using heterogeneous photocatalysis (Blake, 2001), such as acetone, aniline, atrazine, benzene, methyl tertiary butyl ether (MTBE), trichloroethane. The process has also been successfully applied for the treatment of organic and inorganic compounds at low concentrations in aqueous solutions (Wold, 1993; Nakajima et al., 2005; Westerhoff et al., 2005; Le-Clech et al., 2006).

During heterogeneous photocatalysis, organic molecules adsorb onto a metal oxide catalyst surface and react with the photoexcited charge carriers (e^- and h^+) or free radicals (e.g., $\cdot OH$) (Ollis et al., 1984; Kormann et al., 1991). The photocatalytic reaction depends on the species of organic molecules adsorbed onto the photocatalyst surface and in aqueous phase, which results in different kinetics of photodegradation. As a critical step in heterogeneous photocatalysis, very few studies investigated the kinetics of organics adsorption on a photocatalyst (Bauer et al., 2001; Vautier et al., 2001; Hu et al., 2003; Yu et al., 2005; Lee et al., 2011; Zhang et al., 2013; Rioja et al., 2014; Lv et al., 2016).

89   Titanium dioxide (TiO_2) is the most commonly used photocatalyst due to its relatively low cost,

90   high stability, and low toxicity (Fujishima et al., 2000; Kumar and Devi, 2011a; Nakata and

91   Fujishima, 2012). Substantial efforts have been devoted to improve the photocatalytic

92   degradation efficiency of TiO_2 through combination with metal ions, non-metal ions, and some

93   2D nanomaterials (Liqiang et al., 2006; Rubio et al., 2013; Lin et al., 2015; Arlos et al., 2016;

94   Lin et al., 2016; Lin et al., 2017b; Lin et al., 2017f; Li and Hu, 2018; Yi et al., 2018; Merenda et

95   al., 2019). These dopants, such as Ag (Harifi and Montazer, 2014), Fe (Asiltürk et al., 2009; Lin

96   et al., 2016), P (Zhang et al., 2012), SiO_2 (Tawkaew and Supothina, 2008), and graphene (oxide)

97   (Lin et al., 2017c; Lin et al., 2017d; Yi et al., 2018), have been proven to be effective to improve

98   the photocatalytic activity. A recent study reported that the boron nitride (BN) nanosheets exhibit

99   unique properties due to the high surface area and the reactive edge structure (Biscarat et al.,

100   2015). Previous study demonstrated that the introduction of BN nanosheets enhanced the

101   separation of electron–hole pairs of TiO_2 and dramatically improved photocatalytic activity of

102   methyl orange under ultraviolet (UV) irradiation (Nasr et al., 2017b).

103   This study aims to investigate the mechanisms and kinetics of adsorption and photocatalytic

104   oxidation of PPCPs using novel photocatalytic composite TiO_2 nanofibers with boron nitride

105   (BN) nanosheets. Combining TiO_2 with BN nanosheets by electrospinning method is anticipated

106   to enhance the separation of e^--h^+ pairs of TiO_2 thus to improve the photocatalytic activity.

107   Ibuprofen, a nonsteroidal anti-inflammatory drug that has been found extensively in wastewater

108   effluents, was used as the target recalcitrant PPCP. The adsorption and degradation of ibuprofen

109   by photolysis and photocatalysis was characterized by a series of analytical methods.

110   Degradation intermediates of ibuprofen were analyzed by a positive ion electrospray ionization–

111   liquid chromatography–tandem mass spectrometry [(+) ESI LC-MS/MS]. Multiple

112   photocatalytic cycles were conducted to evaluate the recyclability and regeneration of the TiO_2-

113   BN nanocomposites for the degradation of ibuprofen.

114

115   **2. Materials and methods**

116   2.1   Materials and characterization

117   A series of BN nanosheets incorporated TiO_2 nanofibers (0, 3%, 5%, 7%, and 10%, weight

118   percentage of BN to the mass of Ti, referred as TiO_2, TB1, TB2, TB3, and TB4, respectively)

119   were synthesized using electrospinning technique as described by Nasr et al. (2017b). UV-Vis

120   absorbance of the nanofibers was measured by a spectrophotometer (DR6000; Hach Company,

121   CO). X-ray diffraction (XRD) measurements were conducted using a PANAlytical Xpert-PRO

122   diffractometer equipped with an X'celerator detector using Ni-filtered Cu-radiation. The specific

123   surface area of the nanocomposites was determined from the nitrogen adsorption–desorption

124   isotherms measured at liquid nitrogen temperature using a Micromeritics ASAP 2010

125   (outgassing conditions: 200 ºC and 12 h). The structure and morphology of the nanocomposite

126   catalysts was characterized by an H-7650 transmission electron microscope (TEM; Hitachi High-

127   Technologies Corp., Pleasanton, CA). The elemental mapping images were taken with a Zeiss

128   EVO HD15 microscope coupled with an Oxford X-MaxN EDX detector.

129

130   2.2   Adsorption and photodegradation experiments

131   Ibuprofen (Analytical grade; Acros Organics Co, NJ) was used as a model compound

132   representative of PPCPs to evaluate the adsorption and photocatalytic activity of the synthesized

133   nanocomposites. The pH of the tested ibuprofen solution was neutral throughout the experiments.

134   Batch experiments were conducted in 100 mL beakers containing a suspension of 10 mg

135   nanofibers and 50 mL ibuprofen solution (5 mg L^{-1}) under dark (adsorption), UV light

136   irradiation with nanofibers (photocatalysis) or without nanofibers (photolysis) conditions. The

137   irradiance of UV lamp (160W PUV-10, Zoo Med Laboratories, San Luis Obispo, CA) included

138   both UV (365 nm, minor peaks at 290, 315, 335 nm) and visible light (405, 435, and 545 nm)

139   wavelength spectrum. The solution mixtures were magnetically stirred for 2 to 3 hours, and 1 mL

140   water samples were taken at 0, 10, 20, 30, 60, 90, 120, and 180 min. The suspensions were then

141   filtered through 0.45 μm cellulose acetate membrane to separate nanofibers for analysis. All

142   adsorption, photolysis, and photocatalytic degradation experiments under each condition were

143   conducted at least two times to ensure the reproducibility of the results.

144   Repeated ibuprofen degradation experiments were conducted for 16 cycles to evaluate the

145   recyclability of the TiO_2-BN nanocomposites under 3-hour UV light irradiation. Because the

146   filtration and the centrifugation were not effective to collect all the nanocomposites from the

147   solution, the suspensions were dried at 80 °C overnight after each degradation experiment to

148   evaporate water from the ibuprofen and nanofibers mixture solution. Fresh ibuprofen solution

149   was then added to the dried nanocomposites to repeat the photocatalytic experiment.

150

151   2.3   Analytical methods

152   The adsorption and degradation of ibuprofen were characterized by a high-performance liquid

153   chromatography (HPLC; PerkinElmer Series 200, CT, USA), UV absorbance at 254 nm (UV_{254}),

154   and dissolved organic carbon (DOC) quantified through a carbon analyzer (Shimadzu TOC-L,

155   Kyoto, Japan). Specific UV absorbance (SUVA) was quantified by dividing the UV_{254} by the

156   corresponding DOC concentration of ibuprofen samples, which indicates the change of aromatic

157   structure of ibuprofen molecules. Fluorescence excitation-emission matrix (FEEM) spectroscopy

158   was used to obtain information on characteristics of ibuprofen and potential degradation

159   products in water samples (Aqualog-UV-800-C; Horiba Instruments Inc., NJ).

160   The intermediate products of the ibuprofen degradation were further investigated using a (+) ESI

161   LC-MS/MS method with an Ultimate 3000 nano-flow LC system coupled to an Orbitrap Fusion

162   mass spectrometer equipped with an Adivon NanoMate nano-electrospray ionization source.

163   The LC solvent system consisted of water with 0.1% formic acid (A) and acetonitrile with 0.1%

164   formic acid (B). The gradient was 2% B at 0 min to 95% B at 60 min with a 10 min 95% B flush

165   and 20 min equilibration between samples. Data-dependent Orbitrap MS2 mass spectra (HCD

166   Energy = 27%, RP = 30000) were collected with a 3-sec cycle time between parent scans (m/z

167   100-1000, RP = 120000). Easy-IC lock mass calibration was used for parent scans. Background

168   ion signals were excluded from tandem mass spectrometry. Accurate mass measurement for

169   parent ions (e.g. <1 part per million, ppm) was used to constrain tandem mass spectral library

170   matching and impart high confidence to the matched results. Tandem mass spectra were searched

171   against the 2017 NIST tandem MS library and only matches within 1 ppm precursor mass

172   tolerance, 0.5 m/z product ion mass tolerance, a reverse match factor > 700, and C# < 13 were

173   considered robust matches.

174

175   2.4   Adsorption and photocatalytic kinetic models

176   Adsorption kinetics are usually governed by film diffusion and intra-particle diffusion (Lu Lin,

177   2014; Xuesong Xu, 2015; Lin et al., 2017g). However, the adsorption kinetics in this study are

178   complex due to the desorption of ibuprofen molecules from nanofibers with weak adsorption

179   bonding energy. Thus, the adsorption capacity and the rate to reach the equilibrium

180   concentration were investigated using a commonly used kinetic model: the pseudo first-order

181   kinetic model.

182   Typically, the performance of TiO_2 photocatalysis is usually characterized by Langmuir–

183   Hinshelwood kinetic model (Turchi and Ollis, 1990; Ollis et al., 1991; Coleman et al., 2000;

184   Tanaka et al., 2000; Houas et al., 2001; Li et al., 2006; Kumar and Devi, 2011b). It describes a

185   pseudo-first-order kinetics when the initial concentration of ibuprofen is low (millimolar) (Houas

186   et al., 2001; Konstantinou and Albanis, 2004) (Eq. 1):

187
$$ln\left(\frac{C_0}{C}\right) = k_{app}t \tag{1}$$

188   where C_0 and C are the initial and real-time ibuprofen concentrations (mg L^{-1}) at time t (min),

189 k_{app} is the apparent pseudo-first-order rate constant (min^{-1}).

190

3. Results and discussion

191

192   3.1   Characterization of the synthesized catalysts

193   As shown in Figure 1, the peaks in XRD spectra were referred to primary anatase TiO_2 phase in

194   the synthesized catalysts with presence of trace amount of rutile TiO_2 phase. Energy dispersive

195   X-ray spectra (EDX) indicated the amounts of elements B and N increased with increasing BN

196   dose in the TiO_2-BN nanocomposites (Nasr et al., 2017a). However, the XRD patterns of TiO_2-

197   BN nanocomposites were similar to the pure TiO_2, suggesting the doping of BN had marginal

198   impact on TiO_2 crystallization during electrospinning process.

199   The elemental mapping images revealed that Ti, O, B and N elements were evenly distributed

200   over the entire area of the synthesized materials (Nasr et al., 2017a). The morphological and

201   structural features of the synthesized materials were examined by TEM as shown in Figure S1.

202   The TiO_2-BN nanocomposites with different BN doses all displayed in a similar fiber form. The

203   crystallite size of the nanofibers can be determined by Scherrer equation (Lin et al., 2017e). The

204   crystallite sizes of the TiO_2-BN nanocomposites increased slightly with the increasing BN dose

205   (24.3-28.7 nm), while the particle size of pure TiO_2 was the smallest of 16.4 nm (Table 1). The

206   increasing trend of grain sizes was also observed by scanning electron microscopy (SEM)

207   images in previous study (Nasr et al., 2017a). This can be attributed to the increase of the

208   solution viscosity induced by inclusion of BN in the electrospinning solution (Nalbandian et al.,

209   2015). This increase revealed the successful incorporation of BN in TiO_2 nanofibers. Besides,

210   previous XPS analysis of TiO_2-BN nanocomposite suggested the formation of chemical B-O-Ti

211   bond between a titanium atom of TiO_2 and a boron atom at the edge of BN in TiO_2-BN

212   nanocomposite (Liu et al., 2017).
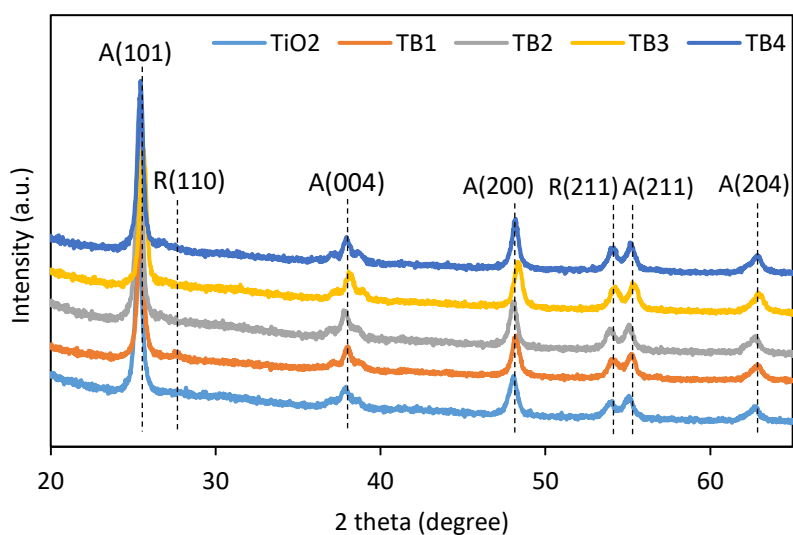
213

214   Figure 1. XRD patterns of synthesized catalysts. A: anatase; R: rutile.

215

216   The specific surface area of the synthesized nanocomposites increased from 19.7 m^2 g^{-1} to 49.6

217 m^2 g^{-1} with the increasing dose of BN nanosheets in the composites (Table 1). In general,

218 materials with a large surface area can accelerate adsorption process due to more active

219 adsorption sites available (Lin et al., 2017a). In addition, the UV-Vis absorption spectra of TiO_2,

220 TB1, TB2, TB3, and TB4 measured in previous study (Nasr et al., 2017a) demonstrated that the

221 incorporation of BN nanosheets improved the light absorbance of the TiO_2-BN nanocomposites

222 in the range of 350-550 nm, which corresponds to the irradiance peak of the UV lamp used in the

223 present work. As such, a higher photocatalytic performance could be expected by combining

224 TiO_2 nanofibers with BN nanosheets. The increased light absorption efficiency resulted in an

225 enhanced photocatalytic activity, which was further evidenced by the degradation of ibuprofen

226 using TiO_2-BN nanocomposites in Section 3.3.

227

228   Table 1. Characterization of the synthesized nanocomposites

| Photocatalysts	TiO_2	TB1	TB2	TB3	TB4
Specific surface area (m^2 g^{-1})	19.7	31.8	34.4	48.3	49.6
Crystalline size (nm)	16.4	24.3	25.2	26.3	28.7

229

230   3.2   Adsorption kinetics of the synthesized catalysts

231 The adsorption kinetics for ibuprofen onto different photocatalysts are shown in Figure 2.

232 Ibuprofen molecules adsorbed onto photocatalysts from the aqueous solution increased quickly

233   over time, and the equilibrium was achieved within 90 min for all photocatalysts. Adsorption

234   onto synthesized nanocomposites showed the same inverted "L" shape, indicating a similar

235   kinetic adsorption process. The adsorption capacity of these catalysts varied in the range of 40-

236   65% after 3-hour adsorption. Ibuprofen had better affinity and higher adsorption with pure TiO_2

237   than with TiO_2-BN nanocomposites.

238   The model parameters and the coefficients of determination (R^2) of the pseudo first-order kinetic

239   equation were calculated based on the experimental data, and the results are summarized in

240   Table 2 (modeling curves are presented in Supporting Information Figure S2). The kinetic model

241   fitted well to the experimental data with the coefficients of determination (R^2) higher than 0.8.

242   The amount of adsorbed ibuprofen at equilibrium (q_e) was approximately 14 mg g^{-1} for all

243   nanocomposites, except for TB4 (10.3 mg g^{-1}). Pure TiO_2 achieved the highest adsorption kinetic

244   rate constant (k_1 = 0.106 min^{-1}), which was 10 times larger than that of TB1. The adsorption

245   kinetic rate constants followed the order of TiO_2 > TB2 > TB3 > TB4 > TB1, which was similar

246   to the tendency observed in Figure 2.
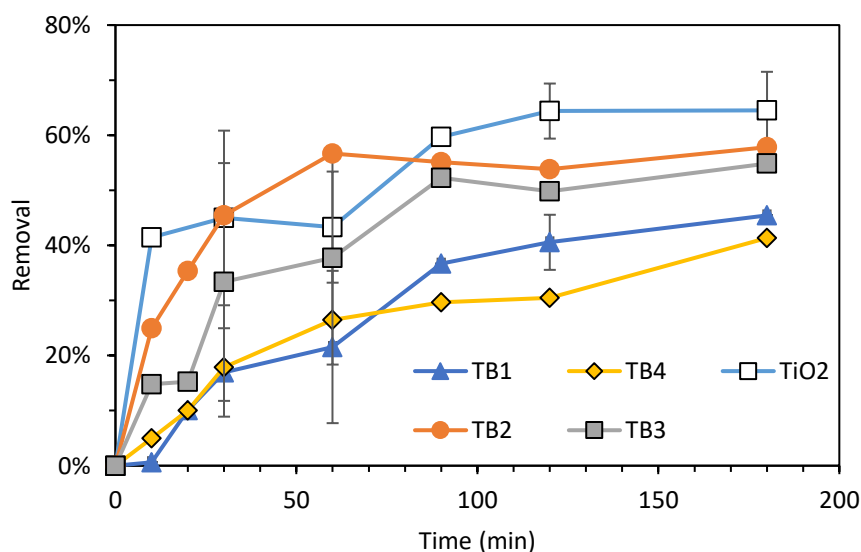
247

248   Figure 2. Adsorption kinetics of ibuprofen onto different photocatalysts. Error bars represent the

249   standard deviation of duplicate experiments.

250

251   Generally, wrapping BN nanosheet onto TiO_2 nanofibers is expected to raise the ibuprofen

252   adsorption onto the photocatalyst due to the larger specific surface area (Table 1). However, the

253   interactions between ibuprofen and the nanocomposite catalysts also govern the adsorption

254   process. Lee *et al.* proposed that the adsorption mechanism between TiO_2 and organics involved

255   the electrostatic (H-bonding) and the covalent (bidentate-bridging mode) bonding (Lee et al.,

256   2011). The surface complex was formed via H-bonding with $TiOH/Ti-OH_2$ (Ti-O) and COO-

257   (COOH) groups (Lee et al., 2011). Besides, ibuprofen is negatively charged with the acid-base

258   logarithmic ionization constant pK_a of 4.85 at neutral pH (Lin et al., 2017a). TiO_2 nanofibers are

259   nearly neutral at pH 7 with the point of zero charge pH_{pzc} of 6.4, while the BN nanosheets are

260   hydrophilic and negatively charged (Lin et al., 2010). As such, the introduction of BN increased

261   the electrical repulsion between ibuprofen and the catalysts, resulting in lower adsorption. In

262   addition, smaller particle size of pure TiO_2 (Table 1) may contribute to higher ibuprofen

263   adsorption because smaller dimension often facilitates adsorption (Yean et al., 2005).

264

265   Table 2. Kinetic parameters for adsorption and photocatalytic activity of the pure TiO_2 and TiO_2-

266   BN nanocomposites

Catalyst	Adsorption			Photocatalysis	
	k_1 (min^{-1})	q_e (mg g^{-1})	R^2	k_{app} (min^{-1})	R^2

TiO$_2$	0.106	14.13	0.836	0.047	0.994
TB1	0.010	13.95	0.974	0.028	0.985
TB2	0.052	14.1	0.996	0.033	0.979
TB3	0.024	13.77	0.964	0.041	0.975
TB4	0.015	10.28	0.974	0.054	0.952

267

268   3.3   Photocatalytic kinetics of the synthesized catalysts

269   The photodegradation of ibuprofen under UV irradiation is shown in Figure 3. The degradation

270   efficiency of direct photolysis (no catalyst) was measured under the same conditions for

271   photocatalysis (with catalyst). After 120 min of UV light exposure, there was 27% degradation

272   of ibuprofen without catalyst. It suggests that ibuprofen molecules can absorb UV light in the

273   region of lamp emission. On the other hand, photodegradation of ibuprofen remarkably improved

274   due to the enhancing effect of the nanocomposites under the UV irradiation. After 2 h of UV

275   light exposure, ibuprofen was almost completely degraded in the presence of photocatalysts.
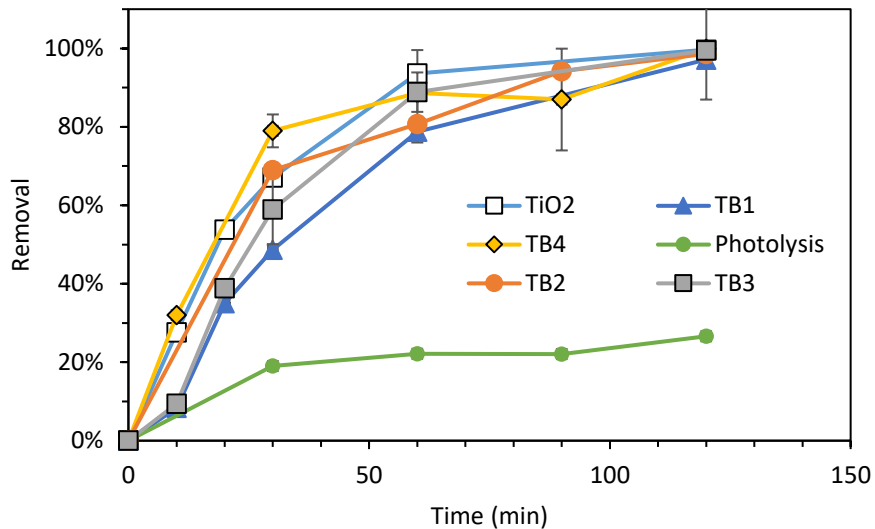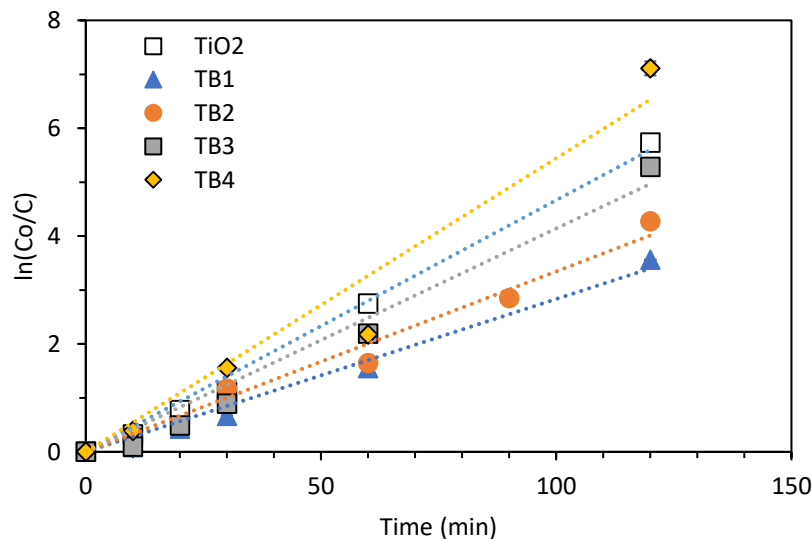
Figure 3. Photocatalytic kinetics of ibuprofen onto different photocatalysts under UV light irradiation. Error bars represent the standard deviation of duplicate experiments.

Langmuir-Hinshelwood kinetic model (Eq. 1) was applied to the photocatalytic data. A plot of $\ln(C_0/C)$ *versus* time t for ibuprofen degradation is presented in Figure 4, and the kinetic parameters are listed in Table 2. The Langmuir–Hinshelwood kinetic model fitted well the experimental data and the coefficients of determination (R^2) obtained were greater than 0.9. The photocatalytic activity presented a similar trend as BN content, except for pure TiO_2. As shown in Table 2, the apparent photocatalysis rate of TB4 (0.054 min^{-1}) was higher than pure TiO_2 (0.047 min^{-1}), while TiO_2 had higher adsorption kinetics rate (TiO_2 0.059 vs. TB4 0.039 min^{-1}). Hence, TB4 exhibits excellent photocatalytic activity for ibuprofen removal rather than adsorption. The photocatalytic degradation rates of TiO_2 and TB2 were lower than adsorption rates, inferring that their adsorption rate is faster than the photocatalytic oxidation rate, so oxidation is the control step for the photocatalytic reaction. On the contrary, adsorption is the

291   control step for TB1, TB3, and TB4 photocatalysis. This was further demonstrated by the

292   multiple photocatalysis cycles discussed in Section 3.6.

293

294   Figure 4. Langmuir-Hinshelwood kinetic modeling curves of ibuprofen degradation by the

295   synthesized nanocomposites

296

297   Adsorption has both positive and negative impacts on photocatalysis. On the one hand, more

298   adsorbed ibuprofen molecules on the catalyst surface improve the transfer of photogenerated

299   radicals, which explained why the photocatalytic degradation rate of TiO_2 was slightly higher

300   than TB1 and TB2. On the other hand, the photocatalytic activity is mainly affected by light

301   absorption capacity and separation efficiency of e^--h^+ pairs. The adsorbed ibuprofen may hinder

302   the photocatalysis degradation by screening the light access to the catalysis, so photocatalytic

303   degradation rate of TiO_2 was relatively low even with the highest adsorption rate. The

304   photocatalytic degradation rate of TiO_2-BN nanocomposite increased with the increasinng BN

305   content probably due to enhanced light absorption intensity (Section 3.1). Meanwhile, due to

306   electrostatic interactions, the negatively charged BN nanosheets surface can lead to the transfer

307   of h^+ from the TiO_2 particles to the BN nanosheets. As such, the recombination of e^- and h^+ is

308   inhibited with increasing BN dose, which was confirmed by previous photoluminescence study

309   (Nasr et al., 2017a).

310

311   3.4   Ibuprofen degradation intermediates and proposed pathway

312   Aiming at identifying the degradation intermediates, (+) ESI LC-MS/MS was performed to

313   detect the constituents in the ibuprofen solutions after photocatalytic treatment. Figure 5 showed

314   extracted-ion chromatographic peak areas for ibuprofen degradation intermediates (including

315   hydroxyibuprofen, carboxyibuprofen, and oxypropyl ibuprofen) after 2-hour UV irradiation. The

316   proposed photocatalytic degradation pathway of ibuprofen is present in Figure 6. All compounds

317   shown were confirmed by high resolution mass spectrometry, where elemental composition of

318   the parent ions was determined from accurate m/z measurement and tandem mass spectrometry

319   indicates molecular structure. For simplicity, only one isomer among several possible is shown at

320   each step. Some intermediates are proposed to be formed by successive free radical

321   hydroxylation followed by oxidation to yield the carbonyl compounds (aldehyde and ketone).

322   The primary carbon oxidation to carboxylic acid is a facile process and that product is confirmed

323   by our mass spectrometry results. The most reactive site of the ibuprofen molecule in the

324   presence of free radical ($^\bullet$OH) is the benzylic carbon, which gives monohydroxylated ibuprofen

325   (confirmed by mass spectrometry). Once the benzylic hydroxyl ibuprofen is formed, it undergoes

326   further oxidation to give the beta-keto acid. Beta keto acids are susceptible for decarboxylation

327   and results the formation of oxypropyl ibuprofen. A similar oxidation decarboxylation route for

328   the degradation of ibuprofen has been reported in the literature (Skoumal et al., 2009).

329   As presented in Figure 3, the sample under direct photolysis (no catalyst) displayed the lowest

330   removal of ibuprofen (27% in 2-hour UV irradiation) and relatively low amounts of degradation

331   intermediates (Figure 5). It suggested only a small fraction of ibuprofen was oxidized and the

332   degradation process was limited to the initial degradation levels. Degradation in the existence of

333   photocatalysts is more complete since both ibuprofen and its degradation products can be

334   adsorbed onto the catalysts. From Figure 3, ibuprofen was almost completely degraded in the

335   presence of photocatalysts after 2-hour UV light exposure, but the amounts of degradation

336   intermediates varied remarkably (Figure 5). Comparing to direct photolysis, the pure TiO_2

337   catalyst showed 27 times, 12 times, and 76 times increase in hydroxyibuprofen,

338   carboxyibuprofen, and oxypropyl ibuprofen, respectively, owing to the degradation of parent

339   compound (ibuprofen). When the BN content increased to 3% (TB1), the amount of degradation

340   intermediates showed 4%, 60%, and 28% reduction relative to the pure TiO_2. The catalysts with

341   5% BN (TB2) also showed a similar increase in degradation intermediates. However, when the

342   BN content increased to 7% (TB3) and 10% (TB4), the degradation intermediates decreased by

343   over 99%, 99%, and 90% for hydroxyibuprofen, carboxyibuprofen, and oxypropyl ibuprofen,

344   respectively, comparing to the pure TiO_2. Hence, the increasing BN content of the catalyst

345   facilitated the breakdown of ibuprofen degradation intermediates. However, the further

346   degradation products were not detected with (+) ESI LC-MS/MS probably due to the low

347   concentration of these compounds. These degradation products with smaller carbon chains might

348   be adsorbed onto the catalysts surface and degraded much faster than ibuprofen and its initial

349   degradation intermediates. More analysis of degradation mechanism was discussed in the

350   following Section 3.5.
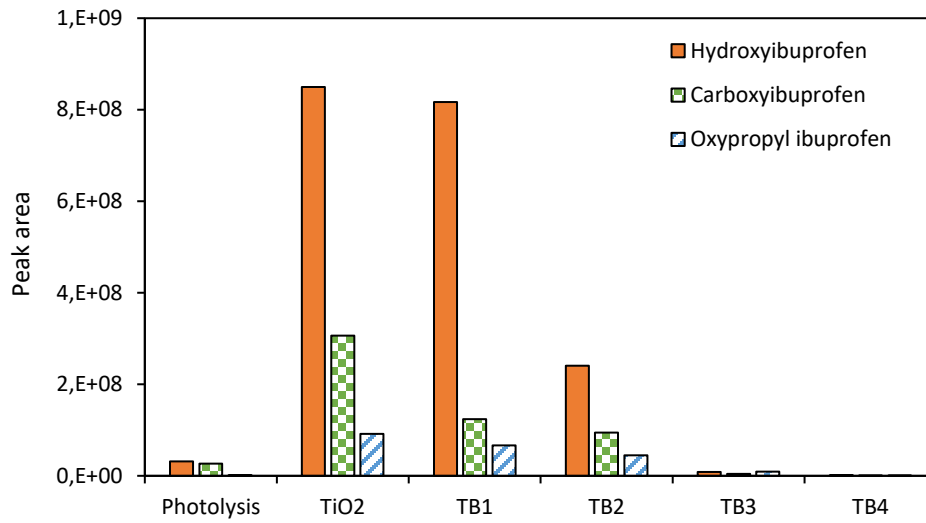
351

Figure 5. Extracted-ion chromatographic peak areas for the precursor masses of ibuprofen

degradation intermediates derived from (+) ESI LC-MS/MS chromatograms from different

catalyst conditions.

355
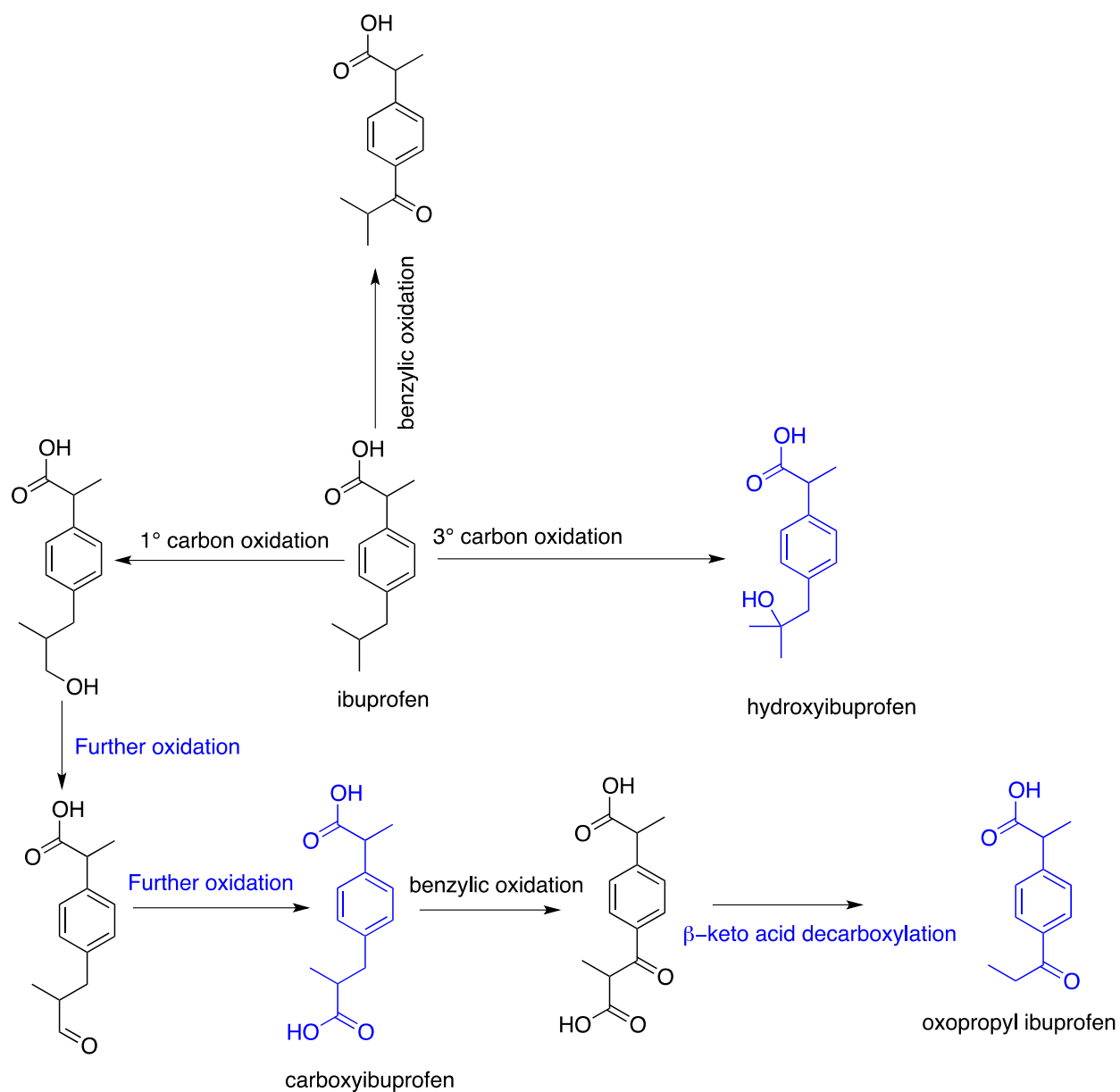
Figure 6. Proposed degradation of ibuprofen by TiO$_2$-BN photocatalysis. Indicated structures were confirmed by mass spectrometry as described.

356

357

358

359   3.5   Photocatalytic oxidation mechanisms of ibuprofen

360   The nanocomposite TB4 was chosen to investigate the photocatalytic degradation mechanism of

361   ibuprofen because of its highest photocatalytic activity among the TiO_2-BN nanocomposites. The

362   photodegradation of ibuprofen was analyzed in terms of HPLC, FEEM, DOC, UV_{254}, and SUVA

363   measurements (Figure 7). The concentration measured by HPLC was the exact concentration of

364   ibuprofen (parent compound); its concentration reduced rapidly and almost completely

365   disappeared after 2-hour reaction. DOC includes all organic carbons in parent compounds,

366   degradation intermediates and products, serving as an indicator for mineralization degree.

367   Compared with the ibuprofen removal results from the HPLC analysis, the DOC reduction was

368   much slower, with only 25% after 2-h reaction. Although the TB4 was effective to oxidize

369   ibuprofen at a fast rate, the organic intermediates from the ibuprofen oxidation need longer time

370   to be mineralized.
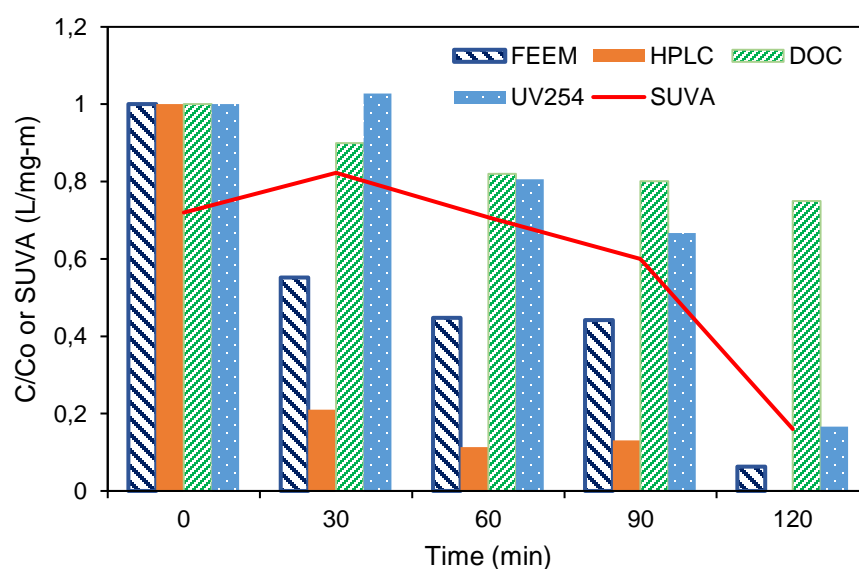
371

372   Figure 7. Reduction of DOC, FEEM peak values, and SUVA values during photocatalytic

373   oxidation of ibuprofen using TB4 under UV irradiation

22

374

375   The UV$_{254}$ and SUVA are used to determine the removal of aromatic fractions of ibuprofen

376   (Stoll et al., 2015). As shown in Figure 7, the SUVA and UV$_{254}$ results exhibited a similar

377   removal trend suggesting aromatic fraction of ibuprofen was degraded. Even though ibuprofen

378   concentration reduced by 79% for the first 30 min, there were 14% and 3% increases in terms of

379   SUVA and UV$_{254}$, respectively. The degradation of ibuprofen was further characterized by the

380   FEEM spectroscopy. The fluorescence peak disappeared after 2-hour of treatment (Figure S3).

381   The excitation-emission peak observed at 220 nm/285 nm corresponds to aromatic compounds

382   (Chen et al., 2003). The fluorescence peak volume was used to compare the aromatic fractions in

383   the tested ibuprofen solution at different reaction time (Figure 7). The peak volume reduced by

384   94% after 2-hour reaction, supporting the decrease in aromatic compounds, consistent with the

385   results of UV$_{254}$ and SUVA that aromatic organic carbon was removed from the solution.

386   The results implied that the intermediates become more aromatic than the parent compound after

387   a partial oxidation. As discussed in Section 3.4, intermediates with more complex structure were

388   detected after photocatalytic treatment. Interestingly, there was only 13% reduction of ibuprofen

389   concentration in the last 30 min of reaction (from 90 to 120 min), but SUVA, UV$_{254}$, and FEEM

390   decreased by 61%, 50%, and 38%, respectively. It suggested that decomposition from parent

391   compounds to intermediates happened mainly during the initial 90 min, while degradation of

392   intermediates into shorter carbon chains occurred mainly after decomposition. Besides, the DOC

393   reduction in the first 30 min probably attributed to the adsorption of ibuprofen onto TB4 (Figure

394   3), the mineralization of ibuprofen was a slow process in the following 90 min due to the tardy

395   reduction of DOC. These results demonstrated that photocatalytic oxidation of ibuprofen

396   molecules by the synthesized nanofibers is a complex multi-step process, degradation of

397   intermediates is probably a control step for the ibuprofen photocatalytic oxidation.

398

399   3.6   Recyclability of the synthesized catalysts

400   The recyclability of the photocatalysts by reusing the catalysts in multiple treatment cycles is

401   crucial in accessing the practical application of a catalyst, because the catalyst may be poisoned

402   by some species (e.g., reaction intermediates) during the reaction process, or may otherwise

403   decompose. In the present work, the recyclability of the pure TiO_2 and TB4 was investigated by

404   performing 16 UV irradiation cycles. In each cycle, UV light was irradiated for 3-hour at room

405   temperature. The adsorption of ibuprofen by TiO_2 and TB4 achieved 65% and 41% after 3-hour

406   mixing (Figure 2), but the photocatalytic activity of TiO_2 and TB4 still remained 80% and 79%

407   after eight cycles of photocatalytic reaction (Figure 8).

408   After eight cycles, the used nanofibers were irradiated by the UV lamp for 3-hour in deionized

409   water. The treatment efficiency was recovered to 98% and 95% for TB4 and TiO_2 after 3-hour

410   regeneration by UV irradiation. However, the degradation efficiency of ibuprofen receded

411   gradually in the following eight cycles, although the TB4 remarkably outperformed TiO_2.

412   According to Section 3.4, more ibuprofen and intermediates were detected for TiO_2 than TB4,

413   hence, weaker photocatalytic activity is probably attributed to the generation and accumulation

414   of intermediates during the catalytic process, which remained on the catalyst and may restrain

415   the further adsorption and degradation of ibuprofen. In addition to the UV irradiation as an

416   effective method for the regeneration of exhausted nanofibers, chemical regeneration should also

417   be studied to fully restore the photocatalysts.
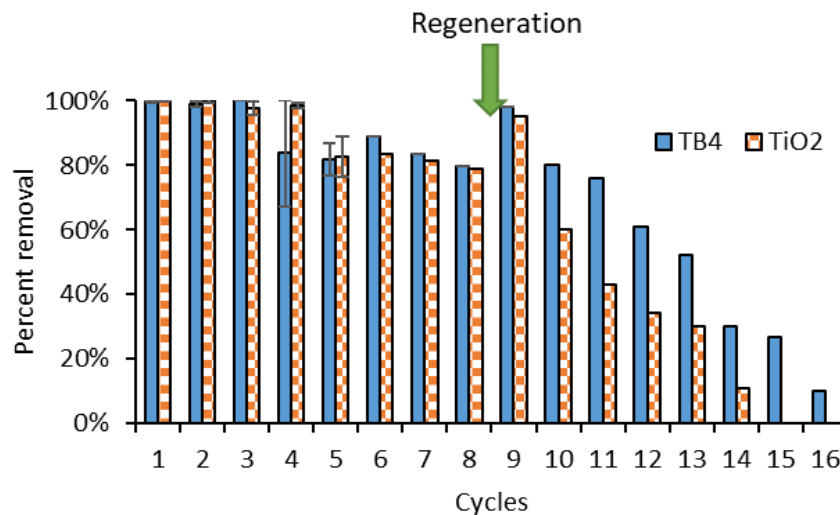
Figure 8. Ibuprofen removal efficiency of TB4 and TiO$_2$ catalysts during multiple photocatalytic cycles under the irradiation of UV light

4. Conclusions

The adsorption, photolysis, and photocatalytic oxidation of ibuprofen by TiO$_2$-BN nanocomposites were studied using a multiple analysis approach. The degradation kinetics, mechanisms, and intermediate products were elucidated. The primary conclusions of the study are summarized as follows.

- Wrapping BN nanosheets onto TiO$_2$ nanofibers improved light absorption efficiency and specific surface area of TiO$_2$ nanofibers, and enhanced separation effectiveness of photogenerated e$^-$-h$^+$ pairs.

- Both adsorption and photocatalytic oxidation of ibuprofen by the TiO$_2$-BN nanocomposites followed the first-order kinetic models. The amount of adsorbed ibuprofen at

432   equilibrium reached approximately 14 mg g^{-1} for the TiO$_2$-BN photocatalysts. The

433   photocatalytic degradation rate increased with the increasing BN content.

434   •   Analysis of degradation intermediates suggested that the increasing BN content of the

435   catalyst facilitated the breakdown of ibuprofen degradation intermediates (hydroxyibuprofen,

436   carboxyibuprofen, and oxypropyl ibuprofen). No further degradation intermediates were detected

437   by the (+) ESI LC-MS/MS chromatograms likely due to lower concentrations of these

438   compounds.

439   •   Multiple photocatalytic cycles were conducted to investigate the reusability of the

440   photocatalysts. UV irradiation of the catalysts in clean water could recover the degradation

441   efficiency to 98% and 95% for TB4 and TiO$_2$. However, photocatalytic activity receded

442   gradually, especially TiO$_2$, as a result of the accumulation of intermediates during the catalytic

443   process. Further chemical regeneration should be investigated to fully recover the photocatalysts.

444   •   Combining TiO$_2$ nanofibers with BN nanosheets provides an innovative method to

445   improve the photocatalytic performance for the degradation of organic contaminants. Further

446   studies on photocatalytic oxidation of organic contaminants of emerging concerns should be

447   conducted using solar light in environmental conditions (e.g., wastewater).

448

453

454

455 **References**

456   Andreozzi, R., Caprio, V., Insola, A., Marotta, R., 1999. Advanced oxidation processes (AOP) for water
457   purification and recovery. Catalysis Today 53, 51-59.
458 Arlos, M.J., Liang, R., Hatat-Fraile, M.M., Bragg, L.M., Zhou, N.Y., Servos, M.R., Andrews, S.A., 2016.
459 Photocatalytic decomposition of selected estrogens and their estrogenic activity by UV-LED irradiated
460 TiO2 immobilized on porous titanium sheets via thermal-chemical oxidation. J Hazard Mater 318, 541-
461 550.
462 Asiltürk, M., Sayılkan, F., Arpaç, E., 2009. Effect of Fe3+ ion doping to TiO2 on the photocatalytic
463 degradation of Malachite Green dye under UV and vis-irradiation. Journal of Photochemistry and
464 Photobiology A: Chemistry 203, 64-71.
465 Bauer, C., Jacques, P., Kalt, A., 2001. Photooxidation of an azo dye induced by visible light incident on
466 the surface of TiO 2. Journal of Photochemistry and Photobiology A: Chemistry 140, 87-92.
467 Biscarat, J., Bechelany, M., Pochat-Bohatier, C., Miele, P., 2015. Graphene-like BN/gelatin
468 nanobiocomposites for gas barrier applications. Nanoscale 7, 613-618.
469 Blake, D., 2001. Bibliography of Work on the Heterogeneous Photocatalytic Removal of Hazardous
470 Compounds from Water and Air--Update Number 4 to October 2001. National Renewable Energy Lab.,
471 Golden, CO (US).
472 Carbonaro, S., Sugihara, M.N., Strathmann, T.J., 2013. Continuous-flow photocatalytic treatment of
473 pharmaceutical micropollutants: Activity, inhibition, and deactivation of TiO2 photocatalysts in
474 wastewater effluent. Applied Catalysis B: Environmental 129, 1-12.
475 Chen, W., Westerhoff, P., Leenheer, J.A., Booksh, K., 2003. Fluorescence Excitation−Emission Matrix
476 Regional Integration to Quantify Spectra for Dissolved Organic Matter. Environmental Science &
477 Technology 37, 5701-5710.
478 Christen, V., Hickmann, S., Rechenberg, B., Fent, K., 2010. Highly active human pharmaceuticals in
479 aquatic systems: A concept for their identification based on their mode of action. Aquatic Toxicology 96,
480 167-181.
481 Coleman, H.M., Eggins, B.R., Byrne, J.A., Palmer, F.L., King, E., 2000. Photocatalytic degradation of 17-β-
482 oestradiol on immobilised TiO2. Appl. Catal., B 24, L1-L5.
483 Dalrymple, O.K., Yeh, D.H., Trotz, M.A., 2007. Removing pharmaceuticals and endocrine-disrupting
484 compounds from wastewater by photocatalysis. Journal of Chemical Technology & Biotechnology 82,
485 121-134.
486 De la Cruz, N., Giménez, J., Esplugas, S., Grandjean, D., De Alencastro, L., Pulgarin, C., 2012. Degradation
487 of 32 emergent contaminants by UV and neutral photo-fenton in domestic wastewater effluent
488 previously treated by activated sludge. water research 46, 1947-1957.
489 De Witte, B., Dewulf, J., Demeestere, K., Van Langenhove, H., 2009. Ozonation and advanced oxidation
490 by the peroxone process of ciprofloxacin in water. Journal of Hazardous Materials 161, 701-708.
491 Doll, T.E., Frimmel, F.H., 2004. Kinetic study of photocatalytic degradation of carbamazepine, clofibric
492 acid, iomeprol and iopromide assisted by different TiO2 materials—determination of intermediates and
493 reaction pathways. Water Research 38, 955-964.
494 Fujishima, A., Rao, T.N., Tryk, D.A., 2000. Titanium dioxide photocatalysis. Journal of Photochemistry and
495 Photobiology C: Photochemistry Reviews 1, 1-21.
496 Harifi, T., Montazer, M., 2014. Fe3+:Ag/TiO2 nanocomposite: Synthesis, characterization and
497 photocatalytic activity under UV and visible light irradiation. Applied Catalysis A: General 473, 104-115.
498 Homem, V., Santos, L., 2011. Degradation and removal methods of antibiotics from aqueous matrices –
499 A review. Journal of Environmental Management 92, 2304-2347.

500 Houas, A., Lachheb, H., Ksibi, M., Elaloui, E., Guillard, C., Herrmann, J.-M., 2001. Photocatalytic
501 degradation pathway of methylene blue in water. Appl. Catal., B 31, 145-157.
502 Hu, C., Tang, Y., Jimmy, C.Y., Wong, P.K., 2003. Photocatalytic degradation of cationic blue X-GRL
503 adsorbed on TiO 2/SiO 2 photocatalyst. Applied Catalysis B: Environmental 40, 131-140.
504 Huerta-Fontela, M., Galceran, M.T., Ventura, F., 2011. Occurrence and removal of pharmaceuticals and
505 hormones through drinking water treatment. Water Research 45, 1432-1442.
506 Jing, L., Qu, Y., Wang, B., Li, S., Jiang, B., Yang, L., Fu, W., Fu, H., Sun, J., 2006. Review of
507 photoluminescence performance of nano-sized semiconductor materials and its relationships with
508 photocatalytic activity. Solar Energy Materials and Solar Cells 90, 1773-1787.
509 Konstantinou, I.K., Albanis, T.A., 2004. TiO2-assisted photocatalytic degradation of azo dyes in aqueous
510 solution: kinetic and mechanistic investigations. Applied Catalysis B: Environmental 49, 1-14.
511 Kormann, C., Bahnemann, D., Hoffmann, M.R., 1991. Photolysis of chloroform and other organic
512 molecules in aqueous titanium dioxide suspensions. Environmental science & technology 25, 494-500.
513 Kumar, S.G., Devi, L.G., 2011a. Review on modified TiO2 photocatalysis under UV/visible light: selected
514 results and related mechanisms on interfacial charge carrier transfer dynamics. J Phys Chem A 115,
515 13211-13241.
516 Kumar, S.G., Devi, L.G., 2011b. Review on modified TiO2 photocatalysis under UV/visible light: selected
517 results and related mechanisms on interfacial charge carrier transfer dynamics. J. Photochem. Photobiol.,
518 A 115, 13211-13241.
519 Le-Clech, P., Lee, E.-K., Chen, V., 2006. Hybrid photocatalysis/membrane treatment for surface waters
520 containing low concentrations of natural organic matters. Water Research 40, 323-330.
521 Lee, C.-R., Kim, H.-S., Jang, I.-H., Im, J.-H., Park, N.-G., 2011. Pseudo First-Order Adsorption Kinetics of
522 N719 Dye on TiO2 Surface. ACS Applied Materials & Interfaces 3, 1953-1957.
523 Lee, Y., von Gunten, U., 2010. Oxidative transformation of micropollutants during municipal wastewater
524 treatment: Comparison of kinetic aspects of selective (chlorine, chlorine dioxide, ferrateVI, and ozone)
525 and non-selective oxidants (hydroxyl radical). Water Research 44, 555-566.
526 Li, S., Hu, J., 2018. Transformation products formation of ciprofloxacin in UVA/LED and UVA/LED/TiO2
527 systems: Impact of natural organic matter characteristics. Water Res 132, 320-330.
528 Li, Y., Li, X., Li, J., Yin, J., 2006. Photocatalytic degradation of methyl orange by TiO2-coated activated
529 carbon and kinetic study. Water Res. 40, 1119-1126.
530 Lin, L., Jiang, W., Xu, P., 2017a. Comparative study on pharmaceuticals adsorption in reclaimed water
531 desalination concentrate using biochar: Impact of salts and organic matter. Sci Total Environ 601-602,
532 857-864.
533 Lin, L., Wang, H., Jiang, W., Mkaouar, A.R., Xu, P., 2017b. Comparison study on photocatalytic oxidation
534 of pharmaceuticals by TiO2-Fe and TiO2-reduced graphene oxide nanocomposites immobilized on
535 optical fibers. J Hazard Mater 333, 162-168.
536 Lin, L., Wang, H., Jiang, W., Mkaouar, A.R., Xu, P., 2017c. Comparison study on photocatalytic oxidation
537 of pharmaceuticals by TiO 2-Fe and TiO 2-reduced graphene oxide nanocomposites immobilized on
538 optical fibers. Journal of Hazardous Materials 333, 162-168.
539 Lin, L., Wang, H., Luo, H., Xu, P., 2015. Enhanced photocatalysis using side-glowing optical fibers coated
540 with Fe-doped TiO2 nanocomposite thin films. Journal of Photochemistry and Photobiology A: Chemistry
541 307-308, 88-98.
542 Lin, L., Wang, H., Luo, H., Xu, P., 2016. Photocatalytic Treatment of Desalination Concentrate Using
543 Optical Fibers Coated With Nanostructured Thin Films: Impact of Water Chemistry and Seasonal Climate
544 Variations. Photochem Photobiol 92, 379-387.
545 Lin, L., Wang, H., Xu, P., 2017d. Immobilized TiO2-reduced graphene oxide nanocomposites on optical
546 fibers as high performance photocatalysts for degradation of pharmaceuticals. Chemical Engineering
547 Journal 310, Part 2, 389-398.

548   Lin, L., Wang, H., Xu, P., 2017e. Immobilized TiO 2-reduced graphene oxide nanocomposites on optical
549   fibers as high performance photocatalysts for degradation of pharmaceuticals. Chemical Engineering
550   Journal 310, 389-398.
551   Lin, L., Wang, H., Xu, P., 2017f. Immobilized TiO 2 -reduced graphene oxide nanocomposites on optical
552   fibers as high performance photocatalysts for degradation of pharmaceuticals. Chemical Engineering
553   Journal 310, 389-398.
554   Lin, L., Xu, X., Papelis, C., Xu, P., 2017g. Innovative use of drinking water treatment solids for heavy
555   metals removal from desalination concentrate: Synergistic effect of salts and natural organic matter.
556   Chemical Engineering Research and Design 120, 231-239.
557   Lin, Y., Williams, T.V., Connell, J.W., 2010. Soluble, Exfoliated Hexagonal Boron Nitride Nanosheets. The
558   Journal of Physical Chemistry Letters 1, 277-283.
559   Liqiang, J., Yichun, Q., Baiqi, W., Shudan, L., Baojiang, J., Libin, Y., Wei, F., Honggang, F., Jiazhong, S.,
560   2006. Review of photoluminescence performance of nano-sized semiconductor materials and its
561   relationships with photocatalytic activity. Solar Energy Materials and Solar Cells 90, 1773-1787.
562   Liu, D., Zhang, M., Xie, W., Sun, L., Chen, Y., Lei, W., 2017. Porous BN/TiO2 hybrid nanosheets as highly
563   efficient visible-light-driven photocatalysts. Applied Catalysis B: Environmental 207, 72-78.
564   Lu Lin, X.X., Charalambos Papelis, Tzahi Y. Cath, Pei Xu, 2014. Sorption of metals and metalloids from
565   reverse osmosis concentrate on drinking water treatment solids. Separation and Purification Technology
566   134, 37-45.
567   Lv, Y., Cao, X., Jiang, H., Song, W., Chen, C., Zhao, J., 2016. Rapid photocatalytic debromination on TiO2
568   with in-situ formed copper co-catalyst: Enhanced adsorption and visible light activity. Applied Catalysis B:
569   Environmental 194, 150-156.
570   Merenda, A., Kong, L., Zhu, B., Duke, M.C., Gray, S.R., Dumée, L.F., 2019. Functional Nanoporous
571   Titanium Dioxide for Separation Applications: Synthesis Routes and Properties to Performance Analysis.
572   in: Pannirselvam, M., Shu, L., Griffin, G., Philip, L., Natarajan, A., Hussain, S. (Eds.). Water Scarcity and
573   Ways to Reduce the Impact: Management Strategies and Technologies for Zero Liquid Discharge and
574   Future Smart Cities. Springer International Publishing, Cham, pp. 151-186.
575   Nakajima, T., Xu, Y.-H., Mori, Y., Kishita, M., Takanashi, H., Maeda, S., Ohki, A., 2005. Combined use of
576   photocatalyst and adsorbent for the removal of inorganic arsenic (III) and organoarsenic compounds
577   from aqueous media. Journal of hazardous materials 120, 75-80.
578   Nakata, K., Fujishima, A., 2012. TiO2 photocatalysis: Design and applications. Journal of Photochemistry
579   and Photobiology C: Photochemistry Reviews 13, 169-189.
580   Nalbandian, M.J., Zhang, M., Sanchez, J., Kim, S., Choa, Y.-H., Cwiertny, D.M., Myung, N.V., 2015.
581   Synthesis and optimization of Ag–TiO 2 composite nanofibers for photocatalytic treatment of impaired
582   water sources. Journal of hazardous materials 299, 141-148.
583   Nasr, M., Viter, R., Eid, C., Habchi, R., Miele, P., Bechelany, M., 2017a. Enhanced photocatalytic
584   performance of novel electrospun BN/TiO2composite nanofibers. New J. Chem. 41, 81-89.
585   Nasr, M., Viter, R., Eid, C., Habchi, R., Miele, P., Bechelany, M., 2017b. Enhanced photocatalytic
586   performance of novel electrospun BN/TiO 2 composite nanofibers. New Journal of Chemistry 41, 81-89.
587   Ollis, D.F., Hsiao, C.-Y., Budiman, L., Lee, C.-L., 1984. Heterogeneous photoassisted catalysis: conversions
588   of perchloroethylene, dichloroethane, chloroacetic acids, and chlorobenzenes. Journal of catalysis 88,
589   89-96.
590   Ollis, D.F., Pelizzetti, E., Serpone, N., 1991. Photocatalyzed destruction of water contaminants. Environ.
591   Sci. Technol. 25, 1522-1529.
592   Prieto-Rodriguez, L., Miralles-Cuevas, S., Oller, I., Agüera, A., Puma, G.L., Malato, S., 2012. Treatment of
593   emerging contaminants in wastewater treatment plants (WWTP) effluents by solar photocatalysis using
594   low TiO2 concentrations. Journal of Hazardous Materials 211, 131-137.

595   Rioja, N., Benguria, P., Peñas, F., Zorita, S., 2014. Competitive removal of pharmaceuticals from
596   environmental waters by adsorption and photocatalytic degradation. Environmental Science and
597   Pollution Research 21, 11168-11177.
598   Rosenfeldt, E.J., Linden, K.G., 2004. Degradation of Endocrine Disrupting Chemicals Bisphenol A, Ethinyl
599   Estradiol, and Estradiol during UV Photolysis and Advanced Oxidation Processes. Environmental Science
600   & Technology 38, 5476-5483.
601   Rubio, D., Casanueva, J.F., Nebot, E., 2013. Improving UV seawater disinfection with immobilized TiO2:
602   Study of the viability of photocatalysis (UV254/TiO2) as seawater disinfection technology. Journal of
603   Photochemistry and Photobiology A: Chemistry 271, 16-23.
604   Skoumal, M., Rodríguez, R.M., Cabot, P.L., Centellas, F., Garrido, J.A., Arias, C., Brillas, E., 2009. Electro-
605   Fenton, UVA photoelectro-Fenton and solar photoelectro-Fenton degradation of the drug ibuprofen in
606   acid aqueous medium using platinum and boron-doped diamond anodes. Electrochimica Acta 54, 2077-
607   2085.
608   Stoll, Z.A., Forrestal, C., Ren, Z.J., Xu, P., 2015. Shale gas produced water treatment using innovative
609   microbial capacitive desalination cell. J Hazard Mater 283, 847-855.
610   Tanaka, K., Padermpole, K., Hisanaga, T., 2000. Photocatalytic degradation of commercial azo dyes.
611   Water Res. 34, 327-333.
612   Tawkaew, S., Supothina, S., 2008. Preparation of agglomerated particles of TiO2 and silica-coated
613   magnetic particle. Materials Chemistry and Physics 108, 147-153.
614   Thagard, S.M., Stratton, G.R., Dai, F., Bellona, C.L., Holsen, T.M., Bohl, D.G., Paek, E., Dickenson, E.R.,
615   2016. Plasma-based water treatment: development of a general mechanistic model to estimate the
616   treatability of different types of contaminants. Journal of Physics D: Applied Physics 50, 014003.
617   Turchi, C.S., Ollis, D.F., 1990. Photocatalytic degradation of organic water contaminants: Mechanisms
618   involving hydroxyl radical attack. J. Catal. 122, 178-192.
619   Van Doorslaer, X., Dewulf, J., De Maerschalk, J., Van Langenhove, H., Demeestere, K., 2015.
620   Heterogeneous photocatalysis of moxifloxacin in hospital effluent: Effect of selected matrix constituents.
621   Chemical Engineering Journal 261, 9-16.
622   Vautier, M., Guillard, C., Herrmann, J.-M., 2001. Photocatalytic degradation of dyes in water: case study
623   of indigo and of indigo carmine. Journal of Catalysis 201, 46-59.
624   Vieno, N.M., Härkki, H., Tuhkanen, T., Kronberg, L., 2007. Occurrence of Pharmaceuticals in River Water
625   and Their Elimination in a Pilot-Scale Drinking Water Treatment Plant. Environmental Science &
626   Technology 41, 5077-5084.
627   Wang, H., Heil, D., Ren, Z.J., Xu, P., 2015. Removal and fate of trace organic compounds in microbial fuel
628   cells. Chemosphere 125, 94-101.
629   Westerhoff, P., Yoon, Y., Snyder, S., Wert, E., 2005. Fate of endocrine-disruptor, pharmaceutical, and
630   personal care product chemicals during simulated drinking water treatment processes. Environmental
631   science & technology 39, 6649-6663.
632   Wold, A., 1993. Photocatalytic properties of titanium dioxide (TiO2). Chemistry of Materials 5, 280-283.
633   Xiang, Y., Fang, J., Shang, C., 2016. Kinetics and pathways of ibuprofen degradation by the UV/chlorine
634   advanced oxidation process. Water Res 90, 301-308.
635   Xuesong Xu, L.L., Charalambos Papelis, Maung Myint, Tzahi Y. Cath, Pei Xu, 2015. Use of drinking water
636   treatment solids for arsenate removal from desalination concentrate. Journal of Colloid and Interface
637   Science 455, 252-261.
638   Yean, S., Cong, L., Yavuz, C., Mayo, J., Yu, W., Kan, A., Colvin, V., Tomson, M., 2005. Effect of magnetite
639   particle size on adsorption and desorption of arsenite and arsenate. Journal of Materials Research 20,
640   3255-3264.
641   Yi, Z., Merenda, A., Kong, L., Radenovic, A., Majumder, M., Dumée, L.F., 2018. Single step synthesis of
642   Schottky-like hybrid graphene - titania interfaces for efficient photocatalysis. Scientific Reports 8, 8154.

643   Yu, Y., Yu, J.C., Chan, C.-Y., Che, Y.-K., Zhao, J.-C., Ding, L., Ge, W.-K., Wong, P.-K., 2005. Enhancement of
644   adsorption and photocatalytic activity of TiO2 by using carbon nanotubes for the treatment of azo dye.
645   Applied Catalysis B: Environmental 61, 1-11.
646   Zhang, S., Chen, L., Liu, H., Guo, W., Yang, Y., Guo, Y., Huo, M., 2012. Design of H3PW12O40/TiO2 and
647   Ag/H3PW12O40/TiO2 film-coated optical fiber photoreactor for the degradation of aqueous rhodamine
648   B and 4-nitrophenol under simulated sunlight irradiation. Chemical Engineering Journal 200-202, 300-
649   309.
650   Zhang, Z., Xiao, F., Guo, Y., Wang, S., Liu, Y., 2013. One-pot self-assembled three-dimensional TiO2-
651   graphene hydrogel with improved adsorption capacities and photocatalytic and electrochemical
652   activities. ACS Appl Mater Interfaces 5, 2227-2233.

653

654

List of the Figure Captions

Figure 1. XRD patterns of synthesized catalysts. A: anatase; R: rutile.

Figure 2. Adsorption kinetics of ibuprofen onto different photocatalysts. Error bars represent the standard deviation of duplicate experiments.

Figure 3. Photocatalytic kinetics of ibuprofen onto different photocatalysts under UV light irradiation. Error bars represent the standard deviation of duplicate experiments.

Figure 4. Langmuir-Hinshelwood kinetic modeling curves of ibuprofen degradation by the synthesized nanocomposites

Figure 5. Extracted-ion chromatographic peak areas for the precursor masses of ibuprofen degradation intermediates derived from (+) ESI LC-MS/MS chromatograms from different catalyst conditions.

Figure 6. Proposed degradation of ibuprofen by TiO_2-BN photocatalysis. Indicated structures were confirmed by mass spectrometry as described.

Figure 7. Reduction of DOC, FEEM peak values, and SUVA values during photocatalytic oxidation of ibuprofen using TB4 under UV irradiation

Figure 8. Ibuprofen removal efficiency of TB4 and TiO_2 catalysts during multiple photocatalytic cycles under the irradiation of UV light